Research article

Parametric study on a Bouc-Wen model with degradation features for the study of cyclic behavior of a reinforced concrete frame

Pedro Folhento[1], Rui Barros[2] and Manuel Braz-Césa[3],*

[1] CONSTRUCT, Faculdade de Engenharia da Universidade do Porto (FEUP), PhD student at FEUP, Rua Dr. Roberto Frias, s/n 4200-465 Porto, Portugal
[2] CONSTRUCT, Faculdade de Engenharia da Universidade do Porto (FEUP), Department of Civil Engineering-Structural Division, Rua Dr. Roberto Frias, s/n 4200-465, Porto, Portugal
[3] CONSTRUCT, FEUP. Instituto Politécnico de Bragança-ESTiG, Campus de Santa Apolónia-5300-253 Bragança, Portugal

* Correspondence: Email: brazcesar@ipb.pt.

Abstract: Non-linear behavior in building frame structures is inevitable and expected in moderate to severe seismic events. This behavior tends to be concentrated at the ends of beams and columns of moment-resisting frames. These critical regions, where plastic hinges form, are important for the global stability of the structural system. Depending on the available ductility, these mechanisms are responsible for the permanent deformations that the structure undergoes, leaving the remaining parts of the structural elements in the elastic regime, and hence in the safe zone. The importance of these mechanisms led to the search for an adequate model capable of well-capturing the non-linearity phenomena involved. The development of versatile hysteresis models with degradation features has been the aim of different studies. Hence, this paper presents a parametric study based on a smooth hysteresis model, a further modification to the well-known Bouc-Wen model, developed by Sivaselvan and Reinhorn, with a physical interpretation appropriate to the study of the non-linear behavior of civil engineering structures, particularly, building structures. Furthermore, an optimization procedure is implemented to calibrate the mentioned model's parameters, attempting to replicate the actual cyclic response of a reinforced concrete frame structure. The effect of each parameter in the hysteresis response will help on the understanding and on the possibilities of this kind of model in simulating different types of structural systems or different materials.

Keywords: hysteresis models; parametric study; non-linear behavior; cyclic response; optimization

1. Introduction

Nonlinearities of hysteresis are present in several phenomena of science and technology, such as physics (e.g. plasticity, friction, ferromagnetism, ferroelectricity, superconductivity, adsorption, and desorption, etc.), chemistry, biology, mechanics, even economics and experimental psychology, but particularly in the present scope, in civil engineering [1,2].

According to Visintin [2], hysteresis is regarded as a rate-independent memory effect. Rate independence requires that the couple (input and output) is invariant to any increasing time homeomorphism, meaning that at any instant of time, the output only depends on the range of the restriction of the input and on the order in which values have been attained, being independent of the derivatives of the input, which may even fail to exist. Hysteresis is then a phenomenological concept that is based on experimental data relating to the aforementioned couple.

In reality, the response of structural systems depends always on the rate of the applied load, and when this needs to be considered, viscosity will be introduced. Although generally in seismic response of structures viscosity and hysteresis contribute to the overall energy dissipated by the structure, if the load is applied at a very low rate, the viscosity phenomena can be neglected [3].

Hysteresis models represent constitutive relationships of a structural system or element. These represent a relationship between a couple of two physical quantities, that in the present scope can be resistance-deformation or stress-strain, shear-distortion, force-displacement, and moment-curvature. More realistic hysteresis models are essential to accurately characterize an inelastic response analysis of a structural system subjected to dynamic loads, such as seismic excitations.

Several hysteresis models were created and studied over the years. These models were developed based on how a certain structural system composed of a certain material behaves under lateral cyclic loading. The characterization of the mechanical non-linear behavior of structural components, e.g., structural elements and connections, and the assessment of the seismic response of structural systems (moment frames, braced frames, and shear and masonry walls) constitute the main purpose in the development of these hysteresis models [4].

The non-linear or inelastic behavior that a structural system exhibits when subjected to a dynamic excitation, can be simulated using a special kind of hysteresis model, an empirical hysteresis model. This kind of model, as the name suggests, is based on a phenomenological approach. The hysteresis characteristics observed in experimental tests of a certain structural system are idealized in a hysteresis model capable of expressing the resistance-deformation relations under any loading history with load reversals [5].

The early models in this context were mainly developed based on experimental observations of reinforced concrete (RC) and steel structural members' behavior. The later and recent hysteresis models are focused on more versatile models capable of simulating different structural systems and different materials under diverse loading conditions. Recent works have presented model formulations capable of accurately simulating complex hysteretic phenomena in rate-independent mechanical systems and materials [6,7], and the complex hysteretic response of elastomeric isolation bearings for seismic isolation [8]. Other studies have presented hysteretic models capable of reproducing damage of structural systems and components presenting stiffness and strength degradation [9,10].

Depending on the loading conditions of a structural member, its behavior can be dominated by flexure, shear, or axial deformation. The interaction between these behaviors can be complex and

must be taken into account to obtain more reliable simulations.

These models can be generally divided into two types, polygonal hysteresis models (PHMs) and smooth hysteresis models (SHMs) [11].

The PHMs are based on piecewise linear behavior and driven by real behavioral stages of an element or structure, such as initial or elastic, cracking, yielding, stiffness and strength degradation stages, and crack and gap closures [11]. Many PHMs were developed over the years mostly to simulate the flexure-dominance behavior of structural members (e.g. elastic-perfectly-plastic bilinear model, strength-hardening bilinear model, Clough's model [12], degrading bilinear model [13], modified Clough's model [14], trilinear degrading model [15], Takeda's model [16,17]. Additionally, to account for shear interaction other models have been developed simulating the pinching effect (e.g. slip-type Takeda's model [18], Kabeyasawa et al. model [19], Three-parameter model [20], Costa and Costa model [21], Rodrigues et al. [22].

Smooth hysteresis models present continuous stiffness changes due to yielding but with sharp changes due to unloading and deteriorating behavior [11]. Different SHMs were developed over the years, although the most popular ones are the Bouc-Wen models, which are a set of models including the original and its further modifications. With proper mathematical manipulations, this constitutive model can represent many different empirical behaviors in a phenomenological way, i.e., softening/hardening and smoothly varying hysteresis curves, e.g., stiffness and strength degradation and the pinching effect.

Bouc-Wen models' can be considered as "semi-physical" models since they come from a combination of some physical understanding of the hysteresis system along with some kind of black-box modeling rather than a detailed analysis of the physical behavior of the systems with hysteresis [23]. This model essentially consists of a first-order non-linear differential equation relating an input displacement and an output restoring force in a hysteresis form. With the proper choice/tuning of parameters, it is possible to replicate the response of the model regarding real hysteresis behavior.

One example of the set of Bouc-Wen models is the Sivaselvan and Reinhorn smooth hysteresis model [11,24]. This model was developed based on previous models, viz., Bouc [25], Wen [26,27], Baber and Noori [28], Foliente [29], and Reinhorn et al. [30]. It is a versatile model that carries a physical interpretation that is appropriate to model the non-linear behavior of structural systems and structural components.

In this paper a parametric variation of a smooth hysteresis model based on the works of Sivaselvan and Reinhorn's [11,24] is performed, to evaluate the role of each parameter for further calibration, attempting to emulate the global cyclic behavior of an experimental RC frame structure using a macro model developed in MATLAB [31].

2. Parametric study

2.1. Characteristics of the experimental frame structure

To study the cyclic response of RC frame structures with or without infill masonry walls an experimental campaign was performed at Laboratório Nacional de Engenharia Civil (LNEC) [32].

The RC bare frame structure used in this experimental study is represented in Figure 1a. A constant vertical load of 100 kN is applied at each column, and the structure is submitted to an

increasing cyclical load/displacement pattern, as represented in Figure 1b, at the beam's center level.

The materials used in the experimental frame structure were concrete of the class C20/25, longitudinal steel reinforcement of S400, and transverse reinforcement (stirrups) of S500.

At the critical regions, i.e., location of the expected plastic hinges, near the extremities of the structural members (Figure 1c), adequate concrete confinement is provided by tightening the spacing between the stirrups as detailed in Figure 1d.

(a) General geometry

(b) Lateral displacement law

(c) Location of critical regions

(d) Cross-sections
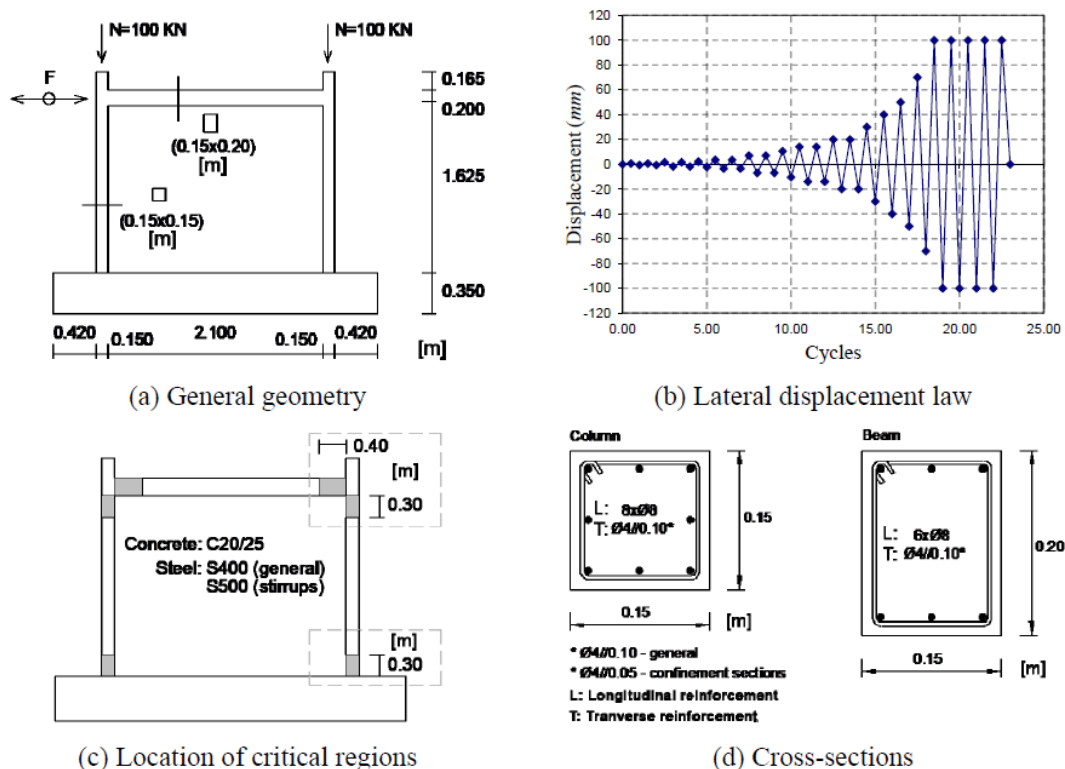
Figure 1. Reinforced concrete frame structure and respective confinement of the critical regions [33].

The experimental model was cyclically loaded in a quasi-statical way by displacement control, according to the displacement law in Figure 1b. Hence, the equation of motion will only comprise the restoring force, which will be further divided into the elastic and inelastic components. Having the displacement that the structure is subjected to and the structure's stiffness, the restoring force can be determined.

The following parametric variation will make use of the structural properties and loading conditions of the described experimental frame structure and testing, presenting all or only specific hysteresis cycles according to the current parameter under study.

2.2. Brief description of the smooth hysteresis model considered

Sivaselvan and Reinhorn developed a polygonal and a smooth hysteresis model [11,24] with degradation features. As mentioned, this modification to the original Bouc-Wen model offers a more physical understanding than preceding modifications since the parameters are selected in a way to

have physical meaning. A brief description of the model used in this study is outlined below based on [11].

The model considered herein comprises three different springs (Figure 2): a post-yielding spring (Spring 1); a hysteresis spring (Spring 2), and a slip-lock spring (Spring 3).
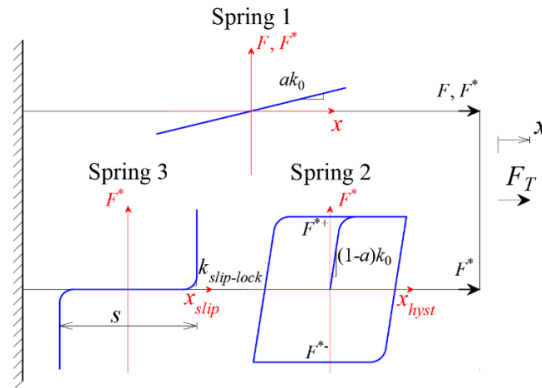

Figure 2. Springs set of the Sivaselvan and Reinhorn's smooth hysteresis model.

MATLAB was used to develop an algorithm to apply the aforementioned model. The differential equation that computes the hysteretic force is given in rate-dependent form as follows [11],

$$\dot{F}^* = k_{hyst}\dot{x} \Leftrightarrow \dot{F}^* = \dot{x}\left(R_K - a\right)k_0\left\{1 - \left|\frac{F^*}{F_Y^*}\right|^N \left[\eta_1 sgn\left(F^*\dot{x}\right) + \eta_2\right]\right\} \tag{1}$$

in which F^* and F^*_Y are the hysteretic force and respective yielding force, x is the total displacement, k_0 is the initial elastic stiffness, k_H is the total non-linear stiffness, k_{hyst} is the hysteretic stiffness, a is the post-yielding to initial stiffness ratio, N is the parameter controlling the smoothness transition from the elastic to the post-yielding range, and η_1 and η_2 are parameters controlling the shape of the unloading path. R_K is related to stiffness degradation, having a positive decreasing value, [11]

$$R_K = \frac{F^* + \alpha F_Y^*}{k_0 x + \alpha F_Y^*} \tag{2}$$

where α controls the degree of stiffness degradation. In addition, stiffness degradation of the elastic spring, i.e., the post-yielding stiffness $k_{post-yield} = ak_0$, can also be considered, as used by other authors [3,34], by the following modification in the elastic spring

$$k_{post-yield,deg} = k_{post-yield}\left[1 - \eta_d\left(\frac{\left|x_{max}^{+/-}\right|}{x_{ult}^{+/-}}\right)\right] \tag{3}$$

The slip lock stiffness, $k_{slip-lock}$, translated by Spring 3 is thus implemented in the model in series with the hysteresis spring to simulate pinching behavior. The combined stiffness can thus be obtained by the following expression [11]

$$k = k_{post\text{-}yield} + \frac{k_{hyst}k_{slip\text{-}lock}}{k_{hyst} + k_{slip\text{-}lock}} \quad \text{where} \quad k_{slip\text{-}lock} = \left\{\sqrt{\frac{2}{\pi}}\frac{s}{\sigma F_Y^*}exp\left[-\frac{1}{2}\left(\frac{F^* - \lambda F_Y^*}{\sigma F_Y^*}\right)^2\right]\right\}^{-1} \tag{4}$$

where s is the slip length, R_s controls the slip length, σ controls the fraction of the yield force beyond which slip will not occur, and λ defines the part of yield force about which slip will occur.

The deterioration of the strength capacity can be simulated by using a rule based on continuous energy degradation and backbone degradation due to the exceeded maximum deformation. This rule can be given by the following expression [11]

$$F_Y^{+/-} = F_{Y0}^{+/-}\left[1 - \left(\frac{x_{max}^{+/-}}{x_{ult}^{+/-}}\right)^{\frac{1}{\beta_1}}\right]\left[1 - \frac{\beta_2}{1-\beta_2}\frac{E_h}{E_{hult}}\right] \tag{5}$$

where $F_Y^{+/-}$ and $F_{Y0}^{+/-}$ are the yield force and the initial yield force, respectively, $x_{max}^{+/-}$ is the maximum displacement, $x_{ult}^{+/-} = x_Y \times \mu_{ult}^{+/-}$ is the ultimate displacement (product between the yield displacement and the ultimate ductility factor), and β_1 and β_2 are parameters based on ductility and energy demands, respectively. The hysteresis energy can be given in incremental form as follows [11]:

$$\Delta E_h = \left[\frac{F + (F + \Delta F)}{2}\right]\left(\Delta x - \frac{\Delta F}{R_K k_0}\right) \tag{6}$$

and the ultimate hysteretic energy under monotonic loading until the ultimate deformation without degradation can be computed by the following expression

$$E_{hult} = \frac{F_{Y0}x_Y}{2} + F_{Y0}\left(x_{ult} - x_Y\right) \tag{7}$$

Asymmetric yielding can also be considered by using the following expression [11]:

$$F_Y^* = (1-a)\left[\left(\frac{1+sgn(\dot{x})}{2}\right)F_Y^+ + \left(\frac{1-sgn(\dot{x})}{2}\right)F_Y^-\right] \tag{8}$$

The experimental model was loaded in a quasi-static cyclic way. Hence, Eq 1 is rewritten for quasi-statically loaded systems, eliminating dt and noting that $sgn(\dot{x}) = sgn(dx)$ [30], considering now the motion independent of time,

$$\frac{dF^*}{dt} = \frac{dx}{dt}(R_K - a)k_0\left\{1 - \left|\frac{F^*}{F_Y^*}\right|^{n_W}\left[\eta_1 sgn\left(F^*\frac{dx}{dt}\right) + \eta_2\right]\right\}$$

$$\Leftrightarrow dF^* = dx(R_K - a)k_0\left\{1 - \left|\frac{F^*}{F_Y^*}\right|^{n_W}\left[\eta_1 sgn\left(F^* dx\right) + \eta_2\right]\right\} \tag{9}$$

and the non-linear equation is solved using a numerical solver such as functions, *fzero*, *fsolve*, or *vpasolve* [31].

2.3. Model parameters variation

The following parametric variation investigates the meaning and the influence of each parameter in the above-presented model. The first graph of Figures 3–13 corresponds to the 18th cycle for different parameter values, and the second plot is the complete hysteretic response for specific parameters' values.

2.3.1. Parameter N

Figure 3 presents the variation of parameter N, controlling the smoothness transition from pre- to the post-yielding range. As can be observed the model becomes approximately bilinear from $N = 15$, showing very little variation between this value and the last one considered ($N = 250$).
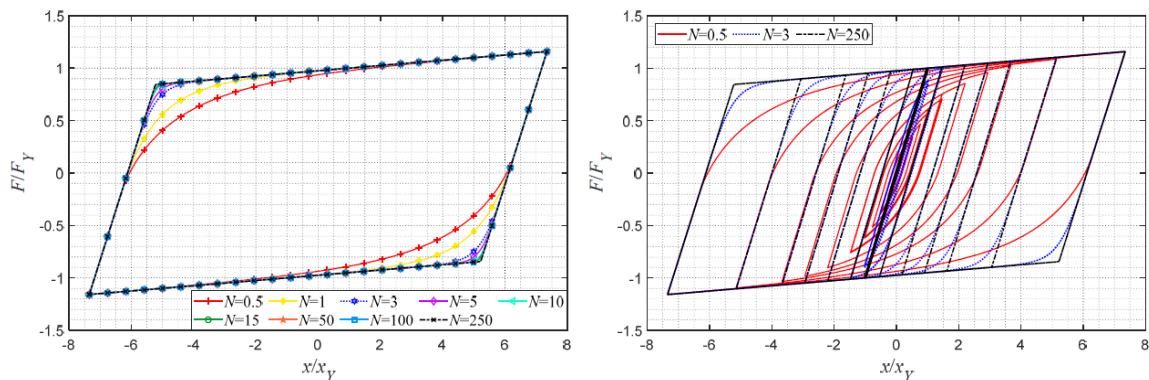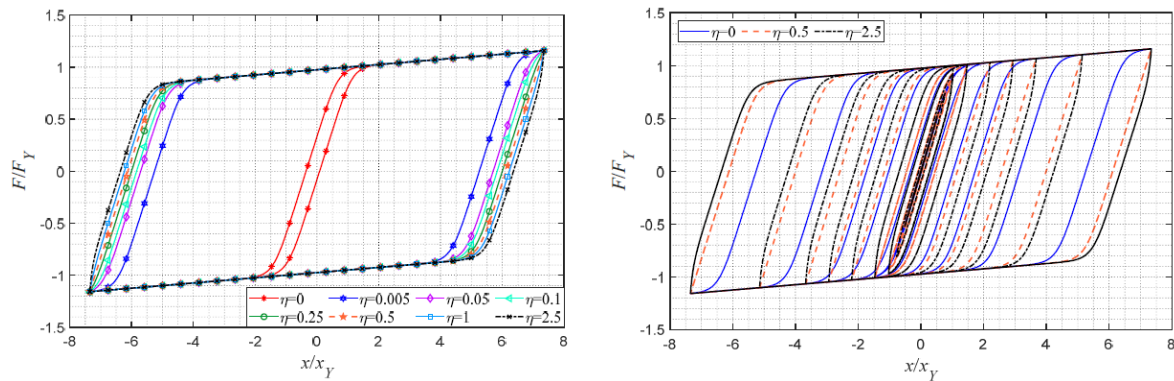

Figure 3. Variation of parameter N ($R_s = 0$, $\sigma = 1$, $\lambda = 0$, $\alpha = 50$, $\eta = 0.5$, $\eta_d = 0$, $a = 0.025$, $\beta_1 = \beta_2 = 0$).

2.3.2. Parameters η_1 and η_2

These two parameters can be reduced to one, η, if one considers the following operation: $\eta_1 + \eta_2 = 1$, leading to [11]:

$$\dot{F}^* = k_{hyst}\dot{x} \Leftrightarrow \dot{F}^* = \dot{x}\left(R_K - a\right)k_0\left\{1 - \left|\frac{F^*}{F_Y^*}\right|^N \left[\eta sgn\left(F^*\dot{x}\right) + \eta - 1\right]\right\}$$ (10)

This is the result of prior studies [35,36], that suggest parameter A (in the original model [26]) is equal to one (Eq 1 and 10) due to redundancies in the model and for mathematical consistency, restoring the physical significance of the initial stiffness; and the previous operation ($\eta_1 + \eta_2 = 1$) is considered for compatibility with plasticity, i.e., returns the physical meaning of the yield force. It should be referred that these values correspond, respectively, to β and γ in the original model [26].

Variation of parameter η is presented in Figure 4 as combinations of η_1 and η_2. It can be verified that this parameter or parameters control the shape of the unloading path, i.e., the variation of the

unloading stiffness, as well as the size of the hysteresis loop, in terms of area and shape. Parameter η will take only positive real values, which corresponds to positive real values for η_1 and positive or negative real values for η_2. When $\eta < 0.5$ the discharge path is linear. For $\eta < 0.5$ the unloading path is non-linear, compressing the loop area, and thus reducing the energy dissipation. For $\eta > 0.5$ the unloading path is also non-linear, although the loop area increases by slightly enlarging the cycle.

Figure 4. Variation of parameter η ($R_s = 0$; $\sigma = 1$; $\lambda = 0$; $\alpha = 100$; $N = 5$; $\eta_d = 0$; $a = 0.025$; $\beta_1 = \beta_2 = 0$).

Other parametric studies [36,37] revealed that if parameters η_1 and η_2 are allowed to vary independently in the context of the original Bouc-Wen model, softening and hardening hysteresis behavior can be obtained for larger and smaller values of η_1, respectively.

2.3.3. Parameters a and η_d

Figures 5 and 6 show, respectively, the variation of the values of parameters a and η_d, while fixing the remaining parameters.
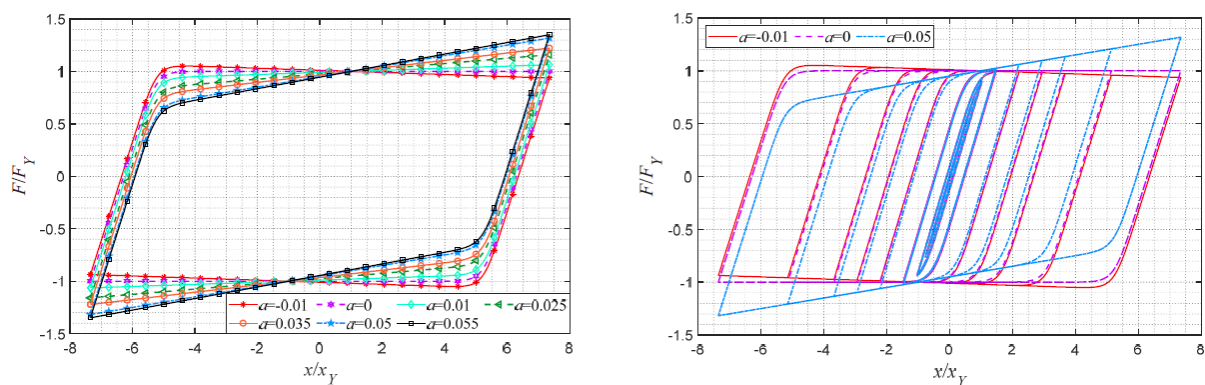

Figure 5. Variation of parameter a ($R_s = 0$, $\sigma = 1$, $\lambda = 0$, $N = 5$, $\eta = 0.5$, $\eta_d = 0$, $\alpha = 100$, $\beta_1 = \beta_2 = 0$).
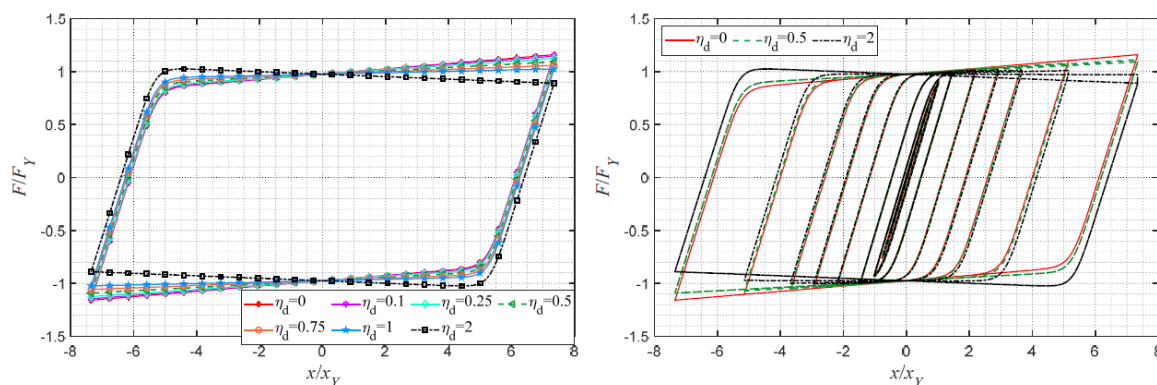
Figure 6. Variation of parameter η_d ($R_s = 0$, $\sigma = 1$, $\lambda = 0$, $N = 5$, $\eta = 0.5$, $\alpha = 100$, $a = 0.025$, $\beta_1 = \beta_2 = 0$).

As mentioned, parameter a accounts for the value of stiffness after yielding, i.e., in the plastic range. This parameter may be seen as a percentage of the initial elastic stiffness.

Recent studies [38,39] proposed the use of negative values for this parameter, resulting in a strain-softening behavior after yielding. Hence, this variation also accounts for negative values of a.

The effect of a negative value of parameter a leads to a clockwise rotation of the hysteresis loops, which allied to the softening behavior results in an increase of strength capacity at the end of the reloading phase, since this model is a Masing type hysteresis model.

The degradation of the post-yielding stiffness can also be implemented in the model [3,34] using the degradation parameter η_d, whose effect presented in Figure 6 reveals higher degradation for larger values of the maximum displacement and parameter η_d.

2.3.4. Parameter α

Hysteresis stiffness degradation is regulated by parameter α, which takes positive real values. This parameter is implemented in the pivot rule [20], leading to a positive decreasing function, R_k (Eq 2), with the unity as its initial and maximum value.

From Figure 7 it is evident that for larger values of α the less stiffness degradation occurs. For values of α between 50 and 250, stiffness degradation is almost inexistent. Despite the influence in the stiffness of the unloading path, an obvious correlation with the hysteresis energy dissipation is seen by observing the reduced area of the hysteresis loops.

Severe stiffness degradation can be verified for values below $\alpha = 5$. Values of α below 0.5 may not represent results with physical significance.
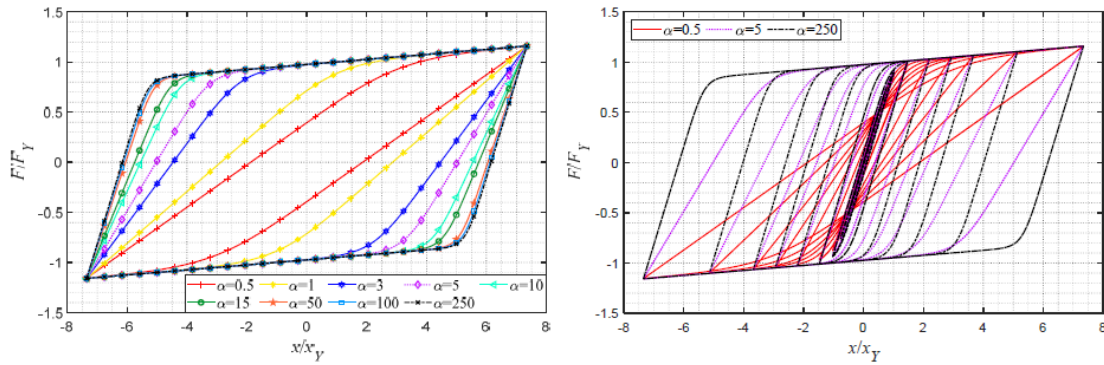
Figure 7. Variation of parameter α ($R_s = 0$, $\sigma = 1$, $\lambda = 0$, $N = 5$, $\eta = 0.5$, $\eta_d = 0$, $a = 0.025$, $\beta_1 = \beta_2 = 0$).

2.3.5. Parameters β_1 and β_2

Figures 8 and 9 show the variation of the parameters controlling the strength deterioration in terms of ductility and energy demands, respectively, β_1 and β_2.
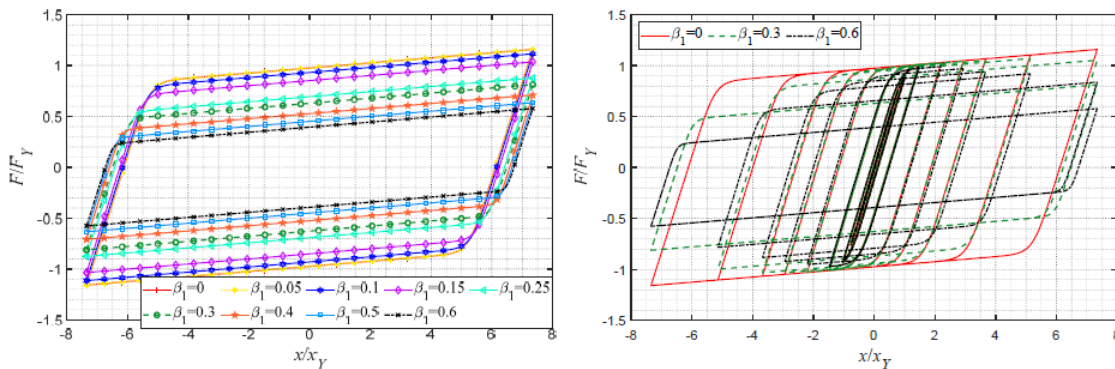

Figure 8. Variation of parameter β_1 ($R_s = 0$, $\sigma = 1$, $\lambda = 0$, $N = 5$, $\alpha = 100$, $\eta = 0.5$, $\eta_d = 0$, $a = 0.025$, $\beta_2 = 0$).
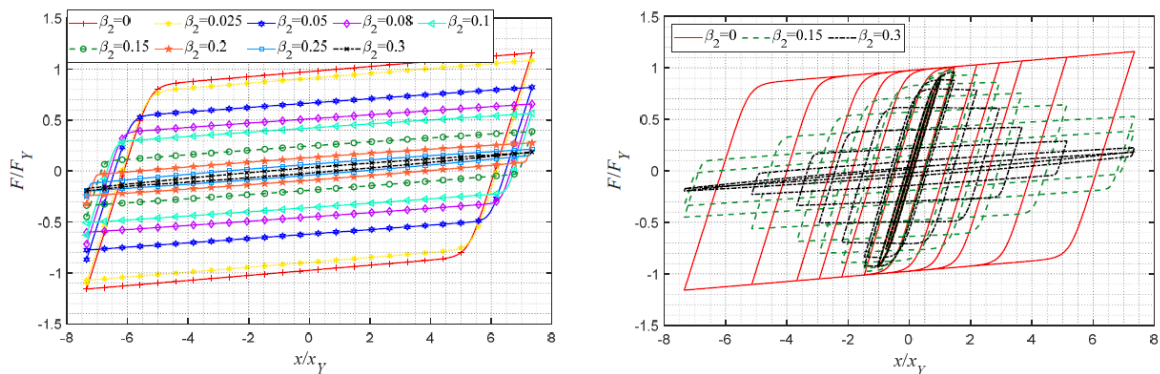
Figure 9. Variation of parameter β_2 ($R_s = 0$; $\sigma = 1$; $\lambda = 0$; $N = 5$; $\alpha = 100$, $\eta = 0.5$; $\eta_d = 0$; $a = 0.025$; $\beta_1 = 0$).

Parameter β_1 depends on the maximum displacement achieved as can be verified by the second term of Eq 5. Hence, whenever a maximum displacement is attained, degradation of the strength capacity occurs by reducing the backbone curve's ordinate. Figure 8 shows severe strength degradation for values between 0.4 and 0.6, and minor strength deterioration for values below 0.1.

Different from β_1, parameter β_2 exhibits continuous resistance degradation based on the incremental energy dissipation. This leads to greater degrees of deterioration for smaller values of β_2 compared with β_1. As can be observed severe resistance degradation can be verified for values of β_2 above 0.15. Values above 0.3 led to numerical instabilities for this case under study.

2.3.6.   Parameters R_s, σ, and λ

In this subsection variation of the parameters' values related to the pinching effect is carried out, viz., parameters R_s, σ and λ.

The slip length s (Figure 2) is regulated by parameter R_s that possess positive real values. The higher the value of R_s the more pronounced the pinching effect is as can be observed by Figure 10. The severe pinching effect can be verified for values bigger than $R_s = 0.4$, and minor pinching effect for very small values of this parameter.
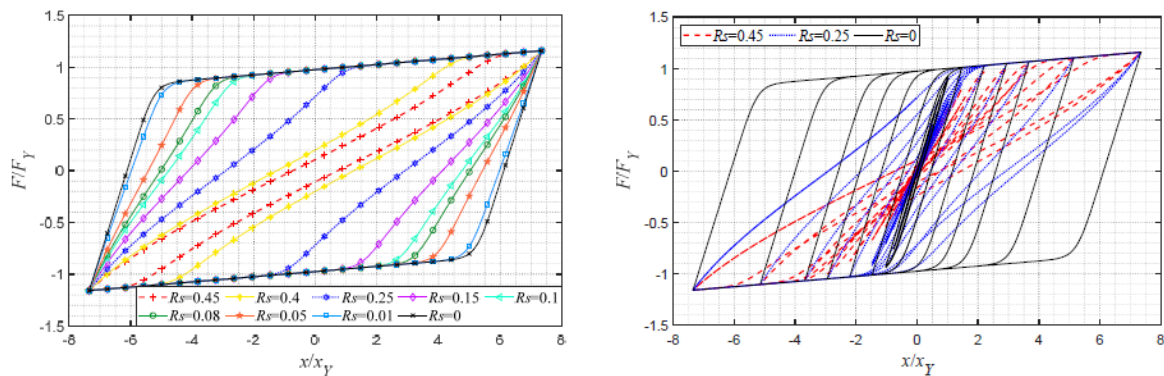

Figure 10. Variation of parameter Rs ($\sigma = 0.75$, $\lambda = 0$, $N = 5$, $\alpha = 100$, $\eta = 0.5$, $\eta_d = 0$, $a = 0.025$, $\beta_1 = \beta_2 = 0$).

The effect of parameter σ is clear by the observation of Figure 11, focusing the pinching effect in a smaller region near the center for smaller values of σ. Slip or the pinching effect will not occur beyond the fraction defined by σ. A value of σ near the unity leads to an almost uniform distribution of the pinching effect in the loading/reloading and unloading branches. Numerical instabilities occur for values of σ very close to zero.
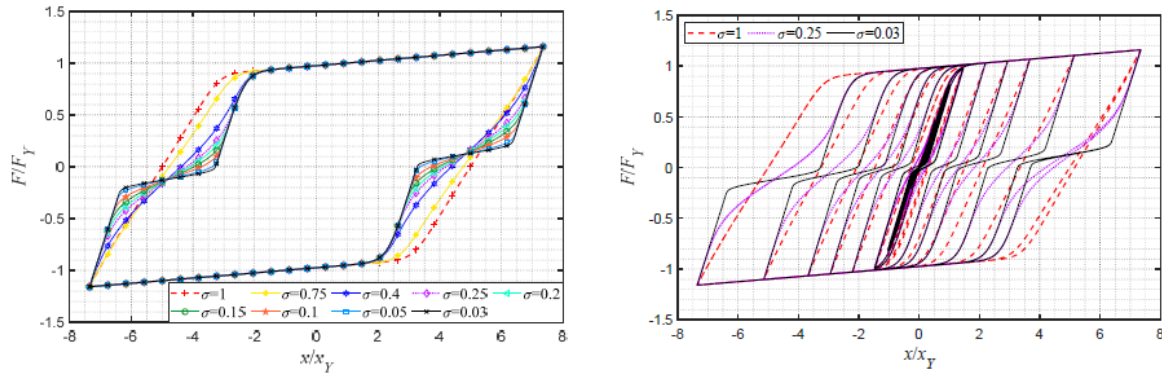
Figure 11. Variation of parameter σ ($R_s = 0.1$, $\lambda = 0$, $N = 5$, $\alpha = 100$, $\eta = 0.5$, $\eta_d = 0$, $a = 0.025$, $\beta_1 = \beta_2 = 0$).

Parameter λ defines the location around which slip will occur. It can take positive or negative real values, and has the positive or negative unity as its maximum or minimum value, respectively. A value different from zero introduces an asymmetric pinching effect in the numerical model. A null value for this parameter means that the structural element or the structure is symmetric. Figure 12 shows the effect of this parameter, which becomes more pronounced for values close to positive or negative one.
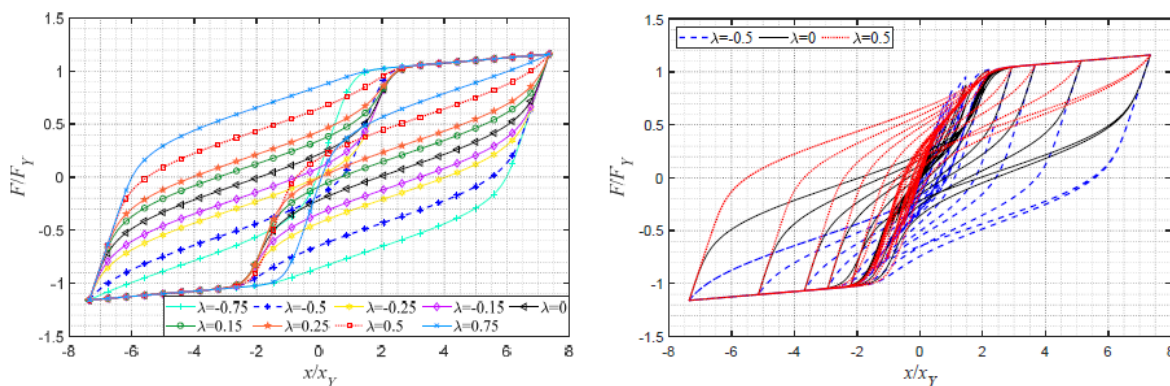

Figure 12. Variation of parameter λ ($R_s = 0.25$, $\sigma = 0.25$, $N = 5$, $\alpha = 50$, $\eta = 0.5$, $\eta_d = 0$, $a = 0.025$, $\beta_1 = \beta_2 = 0$).

2.3.7. Asymmetric yielding

Asymmetric yielding can be considered by the use of Eq 8. Figure 13 shows this feature by varying the yield force in the negative direction to have lower and higher yielding levels than in the positive direction. This feature is important since structural systems are not perfect or ideal, and yielding will possibly have different values in opposite directions.
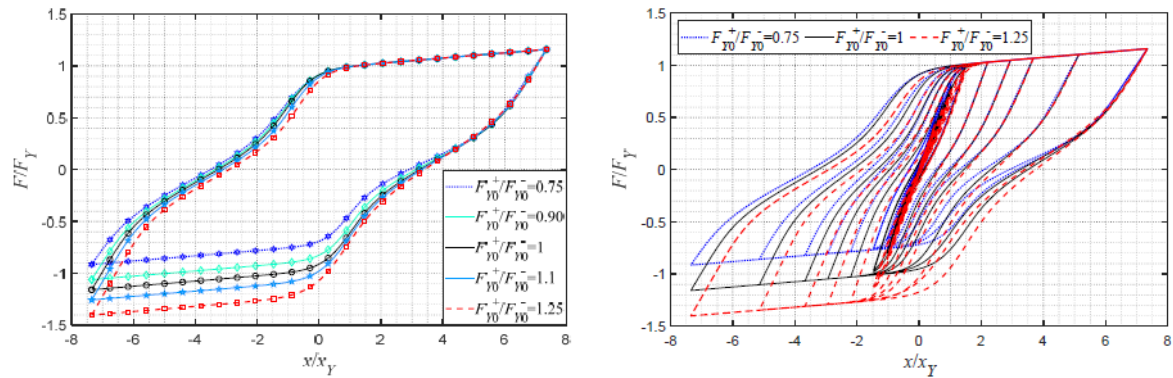
Figure 13. Variation of the yield force in the negative direction ($R_s = 0.1$, $\sigma = 0.25$, $\lambda = 0$, $N = 5$, $\alpha = 5$, $\eta = 0.5$, $\eta_d = 0$, $a = 0.025$, $\beta_1 = \beta_2 = 0$).

3. Calibration of model parameters

The cyclic response of the RC experimental bare frame is presented in Figure 14a. It can be verified a smooth evolution with a subsequent maximum before concrete cracking at the top and bottom ends of the columns. Then, a gradual stiffness decrease occurs without collapse, although with substantial damage, strength deterioration, and inelastic hinge spread in the columns.
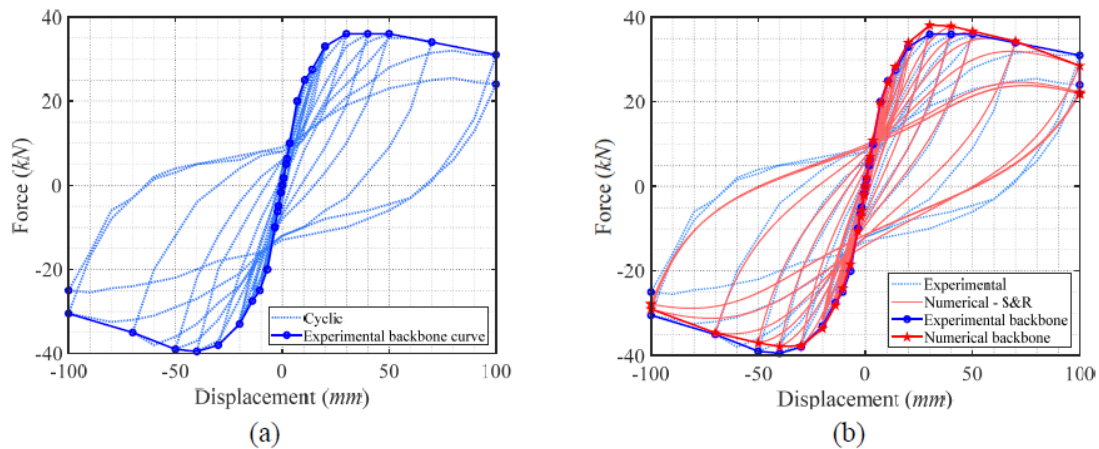

Figure 14. Cyclic response and corresponding backbone curve of the RC frame structure. (a) Experimental, (b) numerical.

Based on the previous parametric study that investigated the influence and effect of each parameter in the hysteresis response, an optimization procedure is carried out to search for the parameters' values that provide the best fit to the experimental data.

The optimal parameters' values defining the smooth hysteresis model that provide the best fitting to the experimental data are obtained by following the procedure illustrated in Figure 15 through a flowchart. The procedure starts with a manual calibration to obtain a starting point or initial guess of the hysteretic parameters for the implementation of function *lsqcurvefit* in MATLAB [31]. This function aims to minimize the sum of squares error between the numerical and

experimental results of the restoring force. The optimized results with this function are then used as an initial guess for the use of function, *fminsearchbnd* [40], based on the *fminsearch* function algorithm [31] that follows the Nelder-Mead simplex algorithm, although with bound constraints applied to the parameters. This function aims to minimize the root mean square error (RMSE) of the same results mentioned, with emphasis given to the points belonging to the cyclic backbone curve through the use of weighting factors. This error was further normalized (NRMSE) with the range of the experimental restoring force and converted to a percentage. The stopping criteria considered for a converged solution were an NRMSE less than 5% and a tolerance less than 1×10^{-4} for the difference between two subsequent iterations on the calculation of the NRMSE.
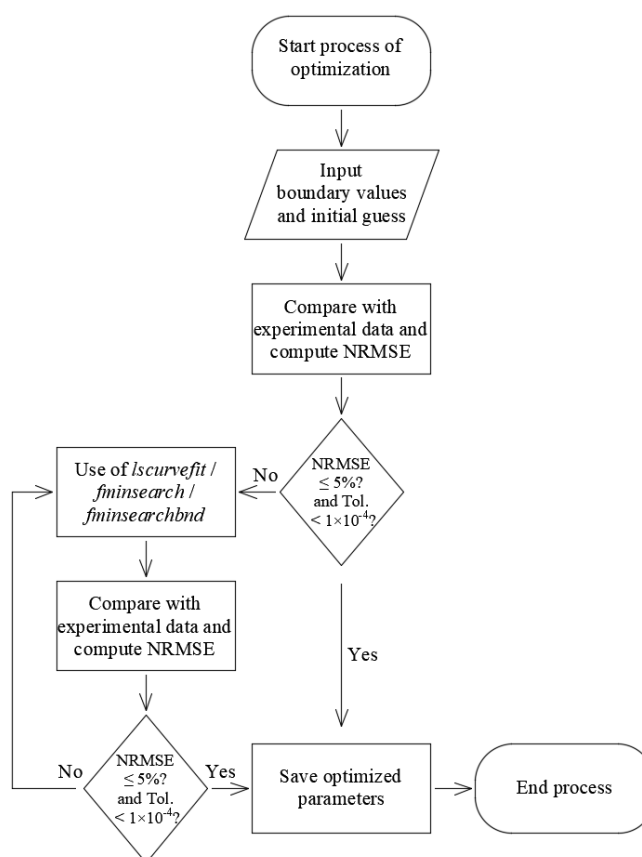

Figure 15. Flowchart of the optimization procedure undertaken in the present study.

The initial stiffness and the yielding force in both directions were also considered in the optimization procedure, verifying that the optimum values are relatively close to the actual values. Figure 14b presents the outcome of the optimization with the following optimized parameters: $N = 2.07$, $a = -0.061$, $\eta_d = 0$, $\eta = 0.81$, $\alpha = 1.33$, $\beta_1 = 0.03$, $\beta_2 = 0.005$, $R_s = 0.17$, $\sigma = 0.40$, $\lambda = 0.004$, $k_0 = 3.567 \times 10^6$ N/m, $F^+_{Y0} = 4.8203 \times 10^4$ N, $F^-_{Y0} = 4.9907 \times 10^4$ N, $\mu^+_{ult} = 7.85$, $\mu^-_{ult} = 14.85$. The model can reasonably estimate the cyclic backbone curve as well as the global hysteretic cycles. The model presents some setbacks in the estimation of the experimental unloading branches and transitions from elastic to plastic range. In addition, further improvements may be applied in the model for the present purpose, viz., in the strength degradation parameters, whose influence and numerical values seem to not correspond to the level of deterioration in the experimental model,

taking very small values. However, the small values of these parameters might be explained by the high degree of stiffness degradation and pinching effect.

The functions used for optimization gave satisfactory results, though a large number of variables were used, exceeding their limit of good performance. As a future development, an optimization procedure should be created to verify if a better solution exists to fit the experimental data.

4. Conclusions

The parametric study performed herein highlighted the importance of each parameter in the hysteresis model investigated. The knowledge of the effect of each parameter in the model provides the necessary insight into the possibilities of the model to estimate real behavior, in the present scope, the non-linear cyclic behavior of RC frame structures.

Based on the parametric study carried out, the calibration of the model's parameters was performed using an optimization procedure to replicate the cyclic behavior of an experimental RC bare frame structure. Satisfactory results were obtained, though a large number of variables were used in the process of optimization, which may compromise the good performance of the implemented functions. Hence, a different optimization approach should be considered to support the current and future solutions.

Further improvements may be carried out for the present purpose, namely, to the strength deterioration formulation to better predict the experimental response, since the values obtained for the corresponding parameters are very small, which may not represent the actual behavior of deterioration. Nevertheless, the level of stiffness degradation and the pinching effect may also explain such low values of the strength deterioration parameters.

Future investigations may comprise validation of the studied hysteresis model with more experimental data considering different hysteretic configurations.

Acknowledgments

Conflict of interest

There is no conflict of interests with the authors and the publication of this paper.

References

1. Krasnosel'skij MA, Pokrovskij AV (1983) *Systems with Hysteresis*, Berlin, Germany: Springer.

2. Visintin A (1994) *Differential Models of Hysteresis. Berlin Heidelberg*, Germany: Springer-Verlag.

3. Apostolos B (2017) Effects of strength hardening, stiffness degradation, strength deterioration and pinching on the seismic response of SDoF systems [Master's thesis]. Delft University of Technology, The Netherlands.

4. Federal Emergency Management Agency (FEMA) (2009) Effects of strength and stiffness degradation on seismic response, P440A, California.

5. Otani S (2002) Nonlinear earthquake response analysis of reinforced concrete buildings. University of Tokyo, Japan.

6. Vaiana N, Sessa S, Marmo F, et al. (2018) A class of uniaxial phenomenological models for simulating hysteretic phenomena in rate-independent mechanical systems and materials. *Nonlinear Dynam* 93: 1647–1669.

7. Vaiana N, Sessa S, Rosati L (2021) A generalized class of uniaxial rate-independent models for simulating asymmetric mechanical hysteresis phenomena. *Mech Syst Signal Pr* 146: 106984.

8. Vaiana N, Capuano R, Sessa S, et al. (2021) Nonlinear dynamic analysis of seismically base-isolated structures by a novel openSees hysteretic material model. *Appl Sci* 11: 900.

9. Do T, Filippou F (2017) A damage model for structures with degrading response. *Earthq Eng Struct D* 47: 311–332.

10. Mazza F (2019) A plastic-damage hysteretic model to reproduce strength stiffness degradation. *B Earthq Eng* 17: 3517–3544.

11. Sivaselvan M, Reinhorn A (2000) Hysteretic models for deteriorating inelastic structures. *J Eng Mech* 126: 633–640.

12. Clough RW (1966) Effects of stiffness degradation on earthquake ductility requirement, UCB/SESM 1966/16, University of California, Berkeley, USA.

13. Nielsen N, Imbeault F (1971) Validity of various hysteretic systems, *Proceedings of the 3rd Japan National Conference on Earthquake Engineering*, 707–714.

14. Otani S (1981) Hysteresis model of reinforced concrete for earthquake response analysis. *J Fac Eng* 36: 407–441.

15. Fukada Y (1969) Study on the restoring force characteristics of reinforced concrete buildings, *Proceedings Kanto Branch Symposium*, Architectural Institute of Japan, 40: 121–124 (in Japanese).

16. Takeda T, Sozen M, Nielsen N (1970) Reinforced concrete response to simulated earthquakes. *J Struct Div* 96: 2557–2573.

17. Takeda T, Sozen MA, Nielsen NN (1971) Reinforced concrete response to simulated earthquakes, OHBAYASHI-GUMI Technical Research Report 5, 19–26, Tokyo, Japan.

18. Eto H, Takeda T (1973) Elasto plastic earthquake response analysis of reinforced concrete frame structure, Architectural Institute of Japan, 1261–1262, Tokyo, Japan (in Japanese).

19. Kabeyasawa T, Shiohara H, Otani S, et al. (1983) Analysis of the full-scale seven-story reinforced concrete test structure. *J Fac Eng* 37: 431–478.

20. Park Y, Reinhorn A, Kunnath S (1987) IDARC: Inelastic Damage Analysis of Reinforced Concrete Frame-Shear-Wall Structures, NCEER-87-0008, National Center for Earthquake Engineering Research, University at Buffalo, State University of New York, Buffalo, New York, USA.

21. Costa AG, Costa AC (1987) Modelo histerético das relações forças-deslocamentos adequado à análise sísmica de estruturas, Laboratório Nacional de Engenharia Civil (LNEC), Lisbon, Portugal.

22. Rodrigues H, Varum H, Costa A (2005) Modelo numérico não-linear para painéis de alvenaria de enchimento em pórticos de betão armado, VII Congreso de Métodos Numéricos en Ingeniería (SEMINI) and IX Congresso Nacional de Mecânica Aplicada e Computacional (APMTAC), 381: 4–7, Granada, Spain.

23. Ismail M, Ikhouane F, Rodellar J (2009) The hysteresis Bouc-Wen model, a survey. *Arch Comput Method E* 16: 161–188.

24. Sivaselvan M, Reinhorn A (1999) Hysteretic models for cyclic behavior of deteriorating inelastic structures, *MCEER-99-0018*, Multidisciplinary Center for Earthquake Engineering Research, New York.

25. Bouc R (1968) Forced vibration of mechanical systems with hysteresis, In: Rupakhety R, Olafsson S, Bessaon B, *Proceedings of the Fourth Conference on Non-linear Oscillation*, Prague: Academia.

26. Wen Y (1976) Method for random vibration of hysteretic systems. *J Eng Mech-ASCE* 102: 249–263.

27. Wen Y (1980) Equivalent linearization for hysteretic system under random excitation. *J Appl Mech* 47: 150–154.

28. Baber TT, Noori MN (1985) Random vibration of degrading pinching systems. *J Eng Mech-ASCE* 11: 1010–1026.

29. Foliente G (1995) Hysteresis modeling of wood joints and structural systems. *J Struct Eng* 121: 1013–1022.

30. Reinhorn A, Mandan A, Valles R, et al. (1995) Modeling of masonry infill panels for structural analysis, NCEER-95-0018, National Center for Earthquake Engineering, USA.

31. The MathWorks, Inc, MATLAB R2019a 9.6.0.1072779, Natick, Massachusetts, USA.

32. Pires F (1990) Influência das paredes de alvenaria no comportamento de estruturas reticuladas de betão armado sujeitas a acções horizontais [PhD Thesis]. LNEC, Lisboa.

33. Braz-César M, Oliveira D, Barros R (2008) Comparison of cyclic response of reinforced concrete infilled frames with experimental results. *14th World Conference on Earthquake Engineering*, Beijing, China.

34. Ray T, Reinhorn A (2014) Enhanced smooth hysteretic model with degrading properties. *J Struct Eng* 140: 04013028.

35. Ma F, Zhang H, Bockstedte A, et al. (2004) Parameter analysis of the differential model of hysteresis. *J Appl Mech* 71: 342–349.

36. Charalampakis A (2010) Parameters of Bouc-Wen hysteretic model revisited. *9th HSTAM International Congress on Mechanics*, Cyprus.

37. Braz-César M, Barros R (2013) Experimental and numerical analysis of MR dampers. *4th ECCOMAS Thematic Conference on Computational Methods in Structural Dynamics and Earthquake Engineering*, Greece.

38. Tsiatas GC, Charalampakis AE (2018) A new hysteretic nonlinear energy sink (HNES). *Commun Nonlinear Sci* 60: 1–11.

39. Charalampakis A, Tsiatas G (2018) Effects of hysteresis and negative stiffness on seismic response rreduction: A case study based on the 1999 Athens, Greece earthquake. *Front Built Environ* 4: 00023.

40. D'Errico J, fminsearchbnd, fminsearchcon. MATLAB Central File Exchange, 2021. Available from: https://www.mathworks.com/matlabcentral/fileexchange/8277-fminsearchbnd-fminsearchcon.